Universiteit
Leiden
The Netherlands

Asyèt yo, Ollas, and Vasijas: situating pottery production in the circum-Caribbean through a technological perspective

Casale, S.

Citation
Casale, S. (2022, December 15). *Asyèt yo, Ollas, and Vasijas: situating pottery production in the circum-Caribbean through a technological perspective*. Retrieved from https://hdl.handle.net/1887/3497642

Version:	Publisher's Version
License:	Licence agreement concerning inclusion of doctoral thesis in the Institutional Repository of the University of Leiden
Downloaded from:	https://hdl.handle.net/1887/3497642

Note: To cite this publication please use the final published version (if applicable).

CHAPTER 2

Geochemical and petrographic assessment of clay outcrops and archaeological ceramics from the pre-Hispanic site of Aguas Buenas (cal 400–1250 CE), central Nicaragua

Simone Casale[1,2], Natalia Donner[1], Dennis Braekmans[1,4,5,6], Alexander Geurds[1,3,7]

1 Faculty of Archaeology, Leiden University, Einsteinweg 2, 2333 CC Leiden, The Netherlands.
2 Royal Netherlands Institute of Southeast Asian and Caribbean Studies, Reuvensplaats 2, 2311 BE Leiden, The Netherlands
3 Institute of Archaeology, University of Oxford, 34-36 Beaumont St, Oxford, OX1 2PG, United Kingdom
4 Cranfield Forensic Institute, Cranfield University, Defence Academy of the United Kingdom, Shrivenham SN6 8LA, United Kingdom
5 Materials Science and Engineering, Delft University of Technology, Mekelweg 2, 2628 CD Delft, The Netherlands
6 Division of Geology, Earth and Environmental Sciences, KU Leuven, Celestijnenlaan 200E, 3001 Heverlee, Belgium
7 Department of Anthropology, University of Colorado-Boulder, 1350 Pleasant Street, Boulder, Colorado 80309, United States

***Microchemical Journal* 156 (2020)** https://doi.org/10.1016/j.microc.2020.104829

ABSTRACT

This research characterizes and reconstructs clay procurement and production practices through the integration of in-situ portable XRF and petrographic analysis on ancient ceramics and clay materials recovered from the Mayales river subbasin (central Nicaragua). A particular choice for this study was the largest and arguably most significant archaeological site in the area, Aguas Buenas (cal 400–1250 CE), a pre-Hispanic indigenous agglomeration consisting of 371 human-made mounds of various shapes arranged in geometric patterns. Microanalytical approaches were applied to reconstruct the use of raw mineral resources in the production of ubiquitous pottery materials found at this site and in its immediate surroundings. The resulting compositional analysis produced geochemical and mineralogical data allowing for the characterisation of distinct, geologically-based compositional groups throughout the valley, improving on the limited geological data resolution previously available. The integrated microscopic and compositional analysis (through p-XRF) of archaeological pottery materials and raw clay samples, generates a number of hypotheses and insights about the nature of the Aguas Buenas site, and its role as a shared space among groups living in the Mayales river subbasin. Additionally, this study provides a solid research framework of investigation that can be employed for more detailed and extensive future studies on pre-Hispanic human occupation in this research area or elsewhere.

Keywords: Archaeological provenance, pre-Hispanic Nicaragua, Petrography, Ceramic microstructure, Geochemical analysis

1. INTRODUCTION

This research aims to define ceramic provenance at a micro-regional scale through the application of both chemical and mineralogical techniques including the use of chemometric approaches. This data is crucial to characterise pre-Hispanic networks of clay procurement practices in the valley of Juigalpa within the Mayales river subbasin (Chontales region, central Nicaragua), with specific attention to the archaeological site of Aguas Buenas. Aguas Buenas is composed of 371 man-made mounds (Geurds et al. 2015; Auzina 2018), making it the largest archaeological site with architectural remains of central Nicaragua, and the most extensive pre-Hispanic site documented in Nicaragua to date. The architectural features are geometrically arranged in an ellipsis that includes six concentric arcs, with a rectangular plaza in the center. Preliminary studies of the site evidence a long biography from 400 to 1200 CE and 1400 to 1600 CE, or the Cuisalá, Potrero and Cuapa phases in the original local chronology (Gorin 1990, Rigat 1992), which is currently under review. Recent detailed mapping and spatial analysis of the site proposed different moments for the construction of Aguas Buenas, which combines various construction preferences resulting in both circular and linear arrangements, alongside clustered structures (Auzina 2019). The area around Aguas Buenas has been the subject of intensive surveying and excavations in recent years (Geurds 2010, 2012, 2013, 2014; Geurds and Terpstra 2017; Vlaskamp, Arteaga 2017; Casale 2017), in the process of which a total of 1671 surface structures were documented distributed across numerous clusters, and in combination with rock art panels (Donner et al. 2018). These 1671 mounds are clustered in 47 different sites in the research area (Fig. 1).

The selected sample of pottery fragments reported here is derived from a large ceramic assemblage excavated from Mound 1 (M1) at Aguas Buenas, which provided macro-fabric, micro-chemical and petrographic variability in a particular "sealed" excavation context estimated to date between cal 400 and 800 CE, according to recent research at the site (Donner and Geurds 2018). As these materials were used in the construction of the mound—both as filling and possibly also as offerings—, they represent choices made over a brief period of time, and therefore represent a suitable opportunity for assessing variability in the human use of clay and ceramic resources at the moment of construction of rows of individual mounds to form concentric arcs—one of the most defining geometric architectural features of the site. In addition, a pedestrian survey, conducted in 2015, aimed to identify clay sources offering reference materials critical to characterize the mineral resources present in the region (Casale et al. 2020), and the possibility to compare these with collected archaeological samples. Chemical analysis by means of portable X-ray fluorescence (p-XRF) combined with principal component analysis (PCA) showed clear chemical variability in clay outcrops, dividing the valley in main geochemical groups. In order to enhance initial results presented in Casale et al.

(2020) and characterise human clay procurement practices as well as technological manufacturing traditions at Aguas Buenas, mineralogical and textural analyses (thin section petrography) were performed, in combination with non-destructive chemical characterisation (by means of in-situ XRF analysis).

This research paper provides the first insights into pre-Hispanic ceramic production in central Nicaragua by integrating data from a pedestrian surface clay survey with microanalytical information. The petrographic and compositional analyses are conducted on the pre-Hispanic ceramic assemblage excavated from M1 at Aguas Buenas, improving the resolution on technological practices at, and beyond, the site. This study improves the capability to establish the provenance of ceramics retrieved at Aguas Buenas, and has a wider impact on the archaeology of central Nicaragua as it provides an initial reference framework for ceramic provenance studies in this region.

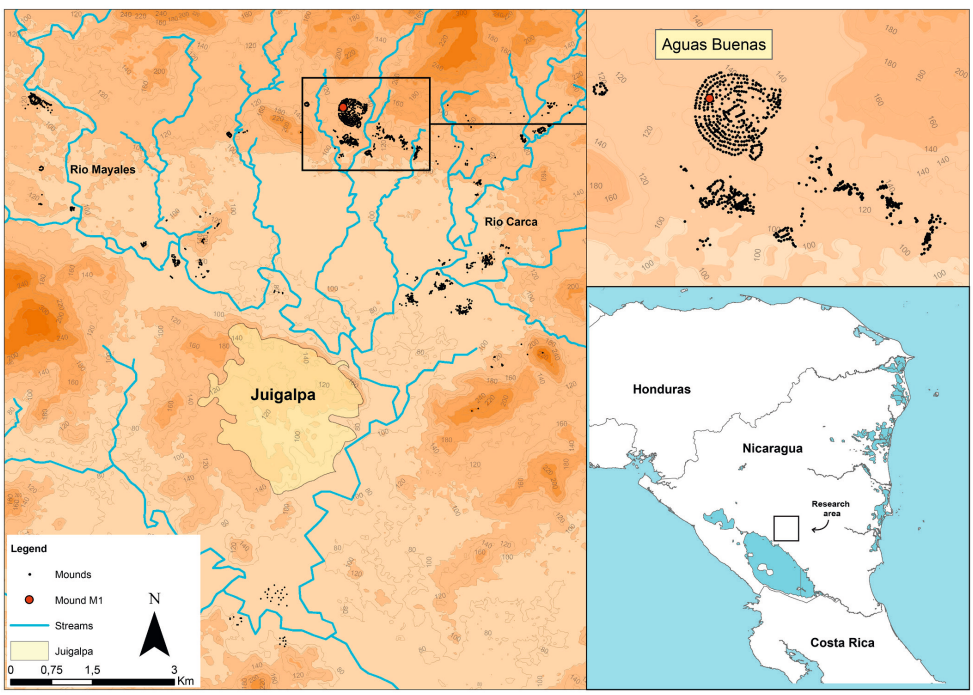

Figure 1. Location of the research area in Central Nicaragua, highlighting Aguas Buenas.

1.1. Geological Context

The research area is located immediately east of the Central Nicaraguan Depression. The Nicaraguan Graben or Depression is the geologically youngest area of Nicaragua and is characterised by a mix of volcanic and sedimentary sequences of Paleocene-Eocene age. The volcanic rocks in this area are mainly composed of porphyritic basalt, basaltic andesite, and andesite to dacitic pumice (Arengi and Hodgson 2000; Hradecký 2011).

The physiography of central Nicaragua includes elevations, plains, large inland lakes, their shores and its islands, as well as the hydrological drainage ultimately leading to the Caribbean Sea (Garayar 1972). The topography of the Mayales river subbasin consists of isolated hills with a plateau shape and soft slopes that are characterised by sharp endpoints. Undulating mountains consist of more recent volcanic rocks, associated with the Tertiary-Quaternary, Coyol group (Late Miocene through the Late Pliocene, possibly up to the Pleistocene); while the eroded slope corresponds to the earlier Matagalpa group (Late Oligocene until Middle Miocene) (Aengi and Hodgson 2000; Garayar 1972). Several large clay deposits have been formed on these geological substrates throughout the entire region. Most of these clay deposits are typically located in the vicinity of rivers and reasonably close to Late Holocene pre-Hispanic settlements, and therefore were likely used as a direct resource for the production of pottery (Casale et al. 2020).

2. MATERIALS AND METHODS

Macro-fabric analysis, thin section petrography and chemical characterisation were applied to a selected dataset of archaeological pottery fragments. The analysis of this study is associated with the results of Casale et al. (Casale et al. 2020) that presented results of p-XRF analysis on raw clay samples collected in the Mayales river subbasin (n=44 samples), and in the Zapatera island (n=5 samples), situated in the Nicaraguan Graben, near the western shore of Lake Cocibolca.

2.1. Sampling of clay and pottery fragments

The ceramic assemblage was obtained through a sampling strategy applied to the entire ceramic collection excavated from Mound M1 at Aguas Buenas. In total, 874 sherds were selected for macro-fabric examination, of which 65% consisted of large fragments (> 5 cm), while the remaining 35% were of smaller dimensions (< 5 cm). Most of the sherds were undecorated or featured a red or brown slip. The results of these macroscopic observations and the established diversity of ceramic paste recipes provided the main rationale for sampling for compositional analysis (see Casale 2017). The description of the sherds was based on five characteristics that are visible with a magnifying glass (10x) and an optical microscope: inclusions, fracture, hardness, compaction, and colour of the matrix. As a result of the macroscopic analysis, 49 archaeological pottery fragments were selected for petrography and, within this group, a subgroup of 30 samples was chosen for compositional analysis. The main goal of the chemical characterisation was to specifically test the possibility of linking the composition of the, (mostly) very coarse, ceramic pastes retrieved at Aguas Buenas, to the available collection of clays, and be able to use this as a baseline and initial reference for future provenance studies and hypothesis testing.

2.2.1. Chemical and petrographic analysis

Based on the provenance postulate, mineralogical and chemical composition of a homogeneous group of ceramics is closely connected to the mineralogical and chemical composition of different clay outcrops used in a production area (Weigand, Harbottle and Sayre 1977). Different analytical techniques such as neutron activation analysis (NAA), inductively coupled plasma mass spectrometry (ICP-MS), X-ray diffraction (XRD) and X-ray fluorescence (XRF) either as Energy Dispersive XRF (ED-XRF) or Wavelength Dispersive XRF (WD-XRF) provide precise compositional results of ceramics and clays and also relating to other archaeological materials such as obsidian, glass, metals and flints (Glascock et al. 1994; Gratuze 1999, Sharrat et al. 2009, Finlay et at. 2012; Guerra 1998; Hughes, Högberg, Olausson 2010; Speakman et al. 2011). However, with the exception of ED-XRF, which also exists in portable version (p-XRF), these techniques are destructive, requiring the extraction of a part of the sample. They are also time consuming and lab-based. As an alternative, p-XRF is non-destructive and expedient for use in the field. The major drawbacks, when compared with lab-based techniques, is that p-XRF has a lower precision to measure low-Z elements, due to the absence of a vacuum that is available for lab-based XRF. It also produces a lower energy X-rays, decreasing the range of elements that can be excited. For quantitative analysis, p-XRF technique has similar limitations to any other XRF devices with ideally the need of a smooth sample surface; a rather homogeneous specimen matrix; and calibration methods that are based on reference materials with matrix similar to the analysed material, allowing users to produce reliable data, in terms of accuracy, precision, and sensitivity. The portable and non-destructive nature of the instrumentation is a major advantage for further field studies with a suitable reference framework in place, however, data analysis needs to be carefully controlled and cautiously interpreted because p-XRF provides semi-quantitative data and it has been the scope of numerous research efforts to ensure reliable data (Shugar and Mass 2012; Morgenstein and Redmount 2005; Frahm 2018; Hunt and Speakman 2015; Emmitt et al, 2018; Pincé et al. 2018). In this research, chemical analysis was carried out by p-XRF, which has been used as an explorative and especially non-destructive technique for provenance studies (Shugar and Mass 2012).

Prior to the analysis, samples were broken and, subsequently, the area of the fresh cut was polished and smoothed with sandpaper to create a clean even surface. To optimize data reliability for each sample, three measurements in different areas were taken to compensate for possible heterogeneity. In general, the ceramics themselves do not show a macroscopically heterogeneous matrix, and occasionally visible larger grains were avoided. As it is shown in section 3.1, the texture of the selected samples is mostly medium coarse, and the average size of inclusions is < 0.5 mm. These characteristics increase the potential of testing for chemical identification of the assemblage, and to compare the results with petrographic observations.

The chemical analysis was conducted using a Bruker Tracer III-SD p-XRF device. The time of analysis was 120 seconds with 40kV and a 14 μA. An Al-Ti-Cu filter was fitted to enhance the instrument's sensitivity in measuring mid-Z trace elements (Rb, Sr, Zr, Y, Nb), following the same methodology used by Casale et al. (2020) to analyse the clay outcrops. Semi-quantitative results were obtained utilizing a custom empirical calibration for ceramic and soil materials. Quality control during analysis was monitored utilizing five rock and soil certified reference materials. These international standards are SRG-1 (Green River Shale), BIR-1 (Icelandic basalt), GSP-2 (Granodiorite Silver Plume), BCR-667 (Estuarine sediments), and CRM NIST-98b (Plastic clay). The following elements were obtained from the analysis: K, Fe, Ca, Ti, Cr, Nb, Ni, Sr, Rb, Y, Zn, and Zr. The elements Fe, Ca, Ti, Cr, Sr, Zr, Rb expressed a $R^2 > 0.90$, as an assessment of accuracy, and were considered for further bi-plots and statistical analysis. Precision—both repeatability and reproducibility—of the measurements was controlled at several instances by replicated analyses and was regularly assessed through the calculation of the relative standard deviation (RSD/%RSD) (Abzalov 2008). All selected elements generated %RSD values below 10% RSD. A table with measured vs. certified values can be found in the supplementary material.

In order to compare and interpret the chemical data of the ceramics, we created bivariate diagrams and additionally used a multivariate statistical approach as classification tools. The use of the multivariate statistical calculations allows for isolating and identifying chemical groups within the assemblage (Baxter 2003). In particular, principal component analysis (PCA) was applied to compare clay raw materials with ceramics and assess possible provenances. Discriminant analysis (DA) using Squared Mahalanobis distances was further used to test the groups created as a result of the petrographic observations and compositional analysis. PCA is additionally a powerful tool to identify which elements contribute to the final composition of the sample. This technique allows for reducing the multivariable dataset to two dimensions, and they are frequently employed to identify subgroups as well as to verify groups created through petrography, stylistic features, or other approaches (VanDerwarker and Marcoux 2019).

For optical mineralogy, thin sections of ceramic fragments were prepared and their structure and composition were observed with a polarizing microscope (Leica DM750P), which uses transmitted plane-polarized (PPL) or cross-polarized (XP) light. The petrographic analysis aimed to characterise the two most important components that constitute a ceramic material: the clay matrix and the non-plastic inclusions. Moreover, it is possible to observe the characteristics of voids, pores, and the presence of slip or paint layers, as well as other types of surface treatment applied by potters (Braekmans and Degryse 2016). The interpretation of these features in comparison with the geological context of the archaeological site from where the materials were excavated, allows us to formulate hypotheses both about provenance, as well as to discriminate materials formed

from different mineral resources (Quinn 2013; Weigand and Harbottle and Sayre 19977). Furthermore, thin section analysis provides information on the employed technological procedures involved in the manufacturing of pottery (Quinn 2013). For instance, through the observation of the birefringence of the clay matrix, it is possible to estimate the firing temperature at which the earthenware was fired. The firing process causes the sintering of the clay components and mineral/rock inclusions, with a loss of 'optical activity' of the matrix. Higher temperature induces important structural changes and the matrix becomes anisotropic, with inclusions that melt and vitrify, creating a more glassy aspect. On average, a clay matrix loses "optical activity" between 800–850 °C. Thus, samples that yield an optical clay matrix are considered to have been fired at temperatures of < 800–850 °C, while those having an inactive matrix are usually fired at temperature > 800–850 °C (Quinn 2013). Photomicrographs were taken with a factory-built Leica camera at the Faculty of Archaeology at Leiden University.

3. RESULTS

3.1. Macroscopic analysis

The assemblage examined included sherds representing different parts of vessels, such as bodies, necks, and rims. Analysis of technological macro traces showed a fashioning technique without the application of rotary kinetic energy, on assembled elements—coils—implying gestures of digital and hand pressure through pinching, drawing, and slight crushing. No percussion was identified, aside from some traces of discontinuous palmar beating. In particular, coils were majorly equidistant, placed alternatively from inside to outside and vice versa. Fashioning was highly homogenous within the entire sample and within the various parts of the vessels, with small variances in coil size, which ranged from 1 to 2 cm. Pre-forming techniques featured a higher variability than in fashioning, with both leather hard (shaving) and wet clay techniques (scraping). For finishing, the microtopography showed horizontal striations linked to brushing and/or smoothing techniques on both wet and leather hard clay. The most commonly applied surface treatment was burnishing; decoration mainly consisted of slips and paint, with a wide range of colors but mostly red, black, red on orange, red on orange on white, red on white, and brown on orange. The high degree of erosion found, together with post-depositional layer attached to the sherd walls and the low firing temperature in some sherds, made macro-trace analysis extremely challenging.

The macroscopic analysis of pastes revealed that inclusions found in the ceramic pastes were coarse, measuring approximately 0.5–1 mm, and their colours varying from white, red, and brown to black. 2% of the sherd assemblage has a highly fine grain matrix (< 0.1 mm), which can be considered as an outlier cluster. In general, the main differences

were in hardness and colour. Variability in the core-margin relationship, cross-section and surface Munsell colors suggests that firing practices involved different temperatures, duration of firing, and position of the vessel (or vessel part) in relation to the fuel source—possibly an open hearth firing context. There may have been an intentional change from oxidizing to reducing firing conditions, based on the current observations. Nevertheless, partially oxidizing firing atmospheres were observed frequently, as identified by a characteristic "sandwich" colouring in the matrix (Orton and Hughes 2013).

A total of 24 homogenous macroscopic clusters were identified, featuring clay recipes that mainly contain feldspars, dark mica, rock fragments, and quartz. These sets of inclusions were repeated in different sizes and frequencies, resulting in a homogenous assemblage comprised of several groups. The orientation of the inclusions was subparallel, concentric, and oblique, and chaotic, which is consistent with the coiling technique for pre-forming vessels (Quinn 2013). Voids were generally of plate-like, oval-sphere, and irregular shapes, and their orientation was also subparallel, concentric, oblique, and chaotic. These macro-groups defined according to their paste characteristics were then used in the secondary sample selection for thin section and compositional analysis.

3.2. Petrographic analysis

A total of 49 sherds was selected for petrographic analysis and subdivided into six petro-groups. A detailed overview of the six petrographic groups identified, and their characteristics, is provided (Table 1, and Figures 2 and 3). Most of the inclusions are connected to a relatively homogeneous mineral composition derived from a basic intermediate igneous parent rock, and in some cases, there are samples with a more mafic (AB-N-45, AB-L-68, AB-D-45) or more andesitic (AB-H-68 and AB-S-78) composition. The ceramic assemblage does not show evidence of calcareous rock inclusions visible through the optical microscope, however, calcareous microscopic inclusions might be present in the matrix as is pointed out by the chemical analysis (see below). The most common inclusions that can be related to these mafic/intermediate rocks are plagioclase, basalt, andesite, pyroxene, olivine, and rarely biotite, as well as hornblende grains. The mineralogy of the inclusions present in the ceramic body is consistent with the geology of the area, which is mainly characterised by Oligocene and mid-Miocene rocks (Arengi and Hodgson 2000).

From a technological perspective, the interpretation of the size, shape and distribution of the inclusions within the matrix suggests that the majority of ceramics were probably not tempered by the intentional grinding of rocks. However, adding temper by re-using ceramic materials (i.e. grog) was an identified practice. Moreover, the matrices of the sherds show evidence of possible mixing of different clays, with at least two clearly distinguishable pastes noted in the same fabric (Fig. 2, caption 11). In particular, it seems

that a lighter, more calcareous fine clay matrix might occasionally have been added to, as indicated, for instance, by samples AB-C-74, AB-A-71X, AB-M-68X, and AB-D-29, however, there is no evidence of medium-coarse rock inclusions of calcareous origin.

The mineralogical characterisation of the samples, examined through thin section petrography, yielded four main compositional clusters (Chontales A, B, C and D). Both petrofabrics C and D have been subdivided to incorporate systematic variations with the respective groups. In total six petrofabrics have been characterized and described.

Chontales A

This fabric is characterised by an orange-brown optically active matrix with an estimated firing temperature lower than 800–850 °C (Quinn 2013). The edges of the samples feature traces of a post-depositional calcite layer and, in a few cases, also a red line below this surface, which may be a trace of finishing and/or surface treatment techniques. The aplastic inclusions show significant variations in dimension. Monocrystalline subangular to subrounded quartz and plagioclase (euhedral and non-euhedral) are the most common inclusions (150–500 µm). There are also medium-coarse sized inclusions (150–600 µm) of chert, granite, basalt and andesite, which vary between subangular and subrounded shapes. The other, much more rare, aplastic inclusions are olivine, orthopyroxene, clinopyroxene, and biotite. The grain size is up to 600 µm, and in a few cases, there are coarse subrounded inclusions of clay pellets and rare grog particles of up to 2000 µm.

Chontales B

Fabric B is characterised by a dark reddish brown optically inactive matrix, suggesting a firing temperature above 850 ℃. The non-plastic inclusions are well-sorted and characterised by a bimodal distribution of fine grains with one range of 150–250 µm and a second range of < 150 µm. Monocrystalline plagioclase and quartz are the most common inclusions. They are characterised by subangular and subrounded shapes. There is a limited number of rock inclusions such as granite, basalt, and chert. Andesite is very rare in these samples. The size of rock inclusions ranges from 150 to 250 µm, with a few isolated inclusions exceeding 500 µm. The other aplastic inclusions are opaque minerals, orthopyroxene, clinopyroxene (augite), and olivine. Their quantity is much lower (< 5%) in comparison to quartz and plagioclase, which comprise 70% of the total inclusions. As with Chontales A, there is a low number of clay pellets and very coarse grog (1000–2000 µm).

Chontales C

Petrographic Fabric C can be defined as the major group in the study. It contains, however, systematic variations that yielded a further subdivision of the ceramics attributed to this petrographic group.

Chontales C-1

This fabric is composed of a non-calcareous orange-yellowish brown slightly optically active matrix, suggesting a firing temperature lower than 800–850 ℃. The outer surface shows traces of a post-depositional layer of calcite. The aplastic inclusions are tri-modal, ranging from 150 to 600 μm. This is a significant size variation, which could be interpreted as an absent or poorly executed sorting strategy. The most common mineral inclusions are quartz, feldspars (k-feldspar and plagioclase crystals) and chert with angular, subangular, subrounded and rounded shapes. There are also minerals of volcanic origin such as orthopyroxene, clinopyroxene (either augite or diopside), olivine, and a very low quantity of large crystals of biotite and hornblende. The rock inclusions are composed of granite and andesite. Basalt occurs in minor quantities and dimensions. A main discriminator is the presence of clay pellets and grog in smaller dimensions (300 and 400 μm) when compared to fabrics A and B.

Chontales C-2

This subgroup consists of a more darkish brown to greyish-brown non-calcareous matrix. The matrix ranges from optically active to inactive, suggesting different firing temperatures from 600 to 800 ℃. Once again, a post-depositional calcite layer covers the surface of the samples a characteristic shared with groups A and C-1. Non-plastic inclusions vary in size, ranging between 150 and 600 μm. Quartz and plagioclase are the main inclusions, followed by granite. There are large coarse inclusions of chert in variable shapes, from subangular to rounded. The other rock inclusions present are basalt and andesite, and these vary from fine to coarse (150–650 μm). Less frequent aplastic inclusions are orthopyroxene and clinopyroxene (augite and rarer diopside), opaque minerals, olivine and (very rare) hornblende and biotite. There are a few isolated cases of large clay pellets (up to 1300 μm), with the average size range being between 300 and 400 μm. The group does not present grog grains.

Chontales D

A further group of samples that shares both technological, matrix and mineralogical features but also exhibit a few differences is group D. Therefore, a subdivision in Group D-1 and D-2 can be defined where D-2 is considered to be the result of mixing multiple raw clay sources, based on the presence of mixing lines in samples (Fig. 2, caption 11), with one of these sources being highly similar as that of the source of Group D-1. The optical activity of the ceramic matrix of these two groups suggests that the vessels were fired at a relatively low temperature < 800–850 ℃.

Chontales D-1

Group D-1 has a light orange-brown optically active matrix. Similar to Groups A, C-1, and C-2, traces of post-depositional calcite were observed on the surface of the sherds. The fabric is characterised by a non-calcareous trimodal matrix, which includes very coarse (1000–2000 μm), coarse (500–1000 μm), and medium (250–500 μm) inclusions. The largest aplastic inclusions are chert (300–1000 μm), granite (200–800 μm), andesite (250–650 μm), and k-feldspars (150–600 μm). The basalt inclusions are smaller (250–300 μm), and either rich or poor in iron content. Quartz and plagioclase are the most common inclusions, and are mostly subangular and subrounded in form. Other inclusions are characterised by single crystals of opaque minerals, orthopyroxene and rare augite (300–150 μm) as well as olivine (150–50 μm), while hornblende and biotite are very rare. The main distinguishing feature, besides the large rock inclusions, is the presence of large grog grains distributed in the matrix (400–1400 μm).

Chontales D-2

The fabric is characterised by a light yellowish-brown matrix, which can be identified as a little more calcareous when compared to groups A, B and C. The distribution of the inclusions is trimodal, characterised by medium and coarse inclusions, which range from 250 to 1000 μm and some very coarse grains measuring between 1200 and 1600 μm. There is a high abundance of coarse chert grains (300–1200 μm) of subangular and subrounded shapes. The other rock inclusions are granite, basalt and andesite from a subangular to subrounded form, which are marked by a significant variation in size (200–1000 μm), suggesting a natural presence of these rocks in the raw sources rather than the addition of temper. Quartz and K-feldspars are the most common inclusions and have a significant variation in dimensions. The quartz pieces vary between 100 and 650 μm and are mostly angular to subangular. The K-feldspars have dimensions between 500 and 1500 μm, while plagioclase, being the most abundant type, measures 150 μm on average. Sanidine is present in minor quantities with dimensions between 700 and 1000 μm. The other inclusions that are present in minor quantities are opaque minerals, orthopyroxene, augite, biotite, and olivine. As in groups A and B, and D-1, grog fragments are also present and vary in dimension (400–500 and 1100–1600 μm). In contrast to groups A and B, clay pellets of very coarse size were not identified.

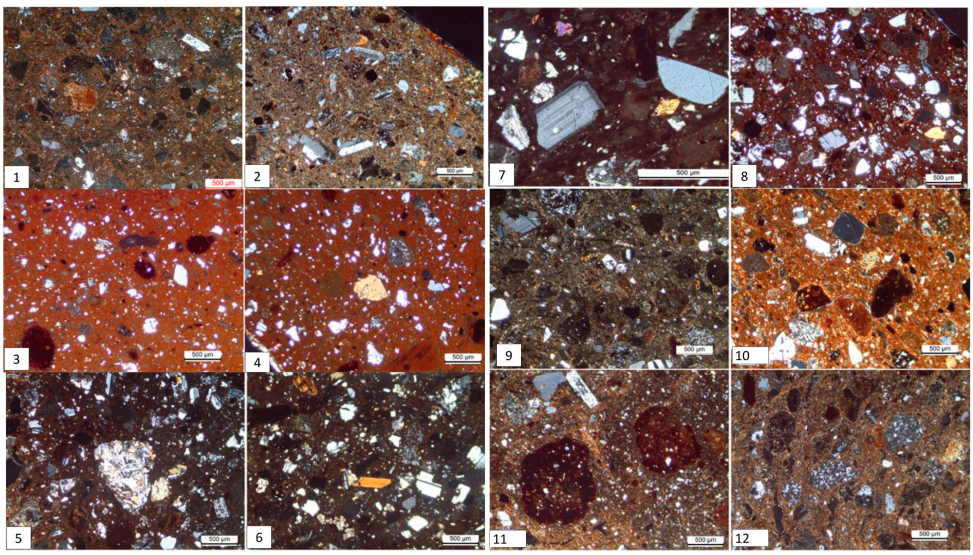

Figure 2. Petrographic groups Chontales A (1 and 2); Chontales B (3 and 4); Chontales C-1(5 and 6); Chontales C-2 (7 and 8); Chontales D-1 9 and 10); Chontales D-2 (11 and 12).

3.3. Chemical analysis

The results of the chemical analysis for the 30 sherds are integrated with the petrographic grouping highlighted in the previous paragraph and shown in Table 2 and Table 3. The scatterplot that compares CaO and Zr (Fig. 3) displays how the values in Zr tend to be heterogeneous throughout the dataset, while there is a correlation between the values of Sr and CaO, which can be associated with the carbonate component of the clays. In contrast, Zr accumulates particularly in coarse and heavy inclusions as a result of high-energy environments, such as river sedimentations (Degryse and Breakmans 2013). As illustrated in the charts (Fig. 3), the petrographic groups are not unequivocally reflected in the chemical composition through these single element observations. In particular, Chontales A (AB-G-71, AB-A-60, AB-P-71, AB-S-78) is characterised by a high correlation in Sr and CaO and a low correlation in Zr (Fig. 3). Samples AB-G-71 and AB-P-71 were also grouped together in the petrographic analysis. The values of Sr and CaO can be associated with the presence of feldspars such as k-feldspar and plagioclase, or their weathering products (Wronkiewicz and Condie 1987) since the carbonate content was exceedingly low in this type of ceramics. These two samples also contain low presence of basalt inclusions. Cr can generate issues in the analysis with p-XRF (Hunt and Speakman 2015), and it was not included in further statistical calculation (see further in the discussion). Chontales B has a composition that can be connected to Chontales A, and only the Cr values are around the detection limit of the p-XRF.

Samples belonging to group Chontales C-1 show lower values in Sr and CaO, which can be related to high levels of sediment weathering, the mobility of these elements,

Table 1. Summary of the petrographic analysis.

Group	Chontales A	Chontales B	Chontales C-1	Chontales C-2	Chontales D-1	Chontales D-2
Samples	AB-O-74;AB-C-74A; AB-R-68X; AB-O-71; AB-F-57; AB-O-68;AB-E-71; AB-H-34; AB-P-42; AB-I-74; AB-F-89; AB-I-83	AB-T-83T; AB-T-60; AB-T-78A	AB-P-71; AB-G-71; AB-M-71; AB-D-78; AB-S-83P	AB-N-60; AB-A-60; AB-Q-89; AB-G-68; AB-F-29; AB-A-71Y; AB-M-68	AB-M-83; AB-A-20; AB-A-71Y; AB-H-78; AB-C-74; AB-I-73	AB-N-45; AB-L- 68; AB-L-78; AB-B-75; AB-P-24; AB-H-68; AB-N-42
Surface treatment	Absent or minor presence of red line (smoothing) below a post-depositional calcite layer	Traces of light grey post-depositional calcite layers, minimum traces	Traces of light grey post-depositional calcite layers, minimum traces or partly covered	Traces of light grey post-depositional calcite layer	Traces of a post-depositional calcite layer of light grey colour	Traces of a light grey post-depositional layer
Matrix (XP)	Orange-brownish, non-calcareous, microcrystalline.	Dark reddish brown, non-calcareous, optically inactive.	An orange-brown to dark reddish brown non-calcareous, slightly optically active.	A dark brown matrix to dark greyish-brown, non-calcareous. From optically inactive to slightly active.	Light orange-brown	Light yellow-brown matrix, non-calcareous.
General inclusion Size	Significant variation, unsorted, 100 µm up to 600 µm. In a few cases >600 µm	Bi-modal, characterized by fine inclusions <150 µm, and more rarely, medium (150-250 µm). Rare exceptions (500-700 µm)	Significant variation, few from 400-600 µm The common sizes are between 250 to 300 µm few (150-300 µm)	Tri-modal characterized by coarse-medium (300-600 µm) and medium (150-250 µm)	Unimodal characterized by very coarse inclusions (1000-2000 µm), coarse (<1 mm) and medium (250-500µm)	Unimodal characterized by medium-coarse (250-800 µm)
Sedimentary rock fragments	Sub-angular and sub rounded chert (300 -500 µm, in a few cases 900-1000 µm)	Very rare chert +/-110 µm	Sub-angular, sub-rounded and rounded chert (250-900 µm)	Sub-angular, sub-rounded and rounded chert with significant variation in dimension (isolate 1700 µm; average 200-700 µm)	Sub-angular, sub-rounded and rounded chert (300-1000 µm)	Sub-angular, sub-rounded and rounded chert (300-1200 µm)

Table 1. Summary of the petrographic analysis. (continued)

Group	Chontales A	Chontales B	Chontales C-1	Chontales C-2	Chontales D-1	Chontales D-2
Igneous Rock fragments	Sub-angular and sub-rounded granite, basalt and andesite (150-600 µm)	Sub-rounded and rounded granite (90-120 µm) and few (200-400 µm), rare andesite.	Sub-angular and sub-rounded granite (200-600 µm), few basalt (200-300 µm) and andesite (250-550 µm)	Sub-angular and sub-rounded granite (200-600 µm) basalt and andesite (150-650 µm)	Sub-angular and sub-rounded granite (200-800 µm), basalt (250-300 µm) and andesite (250-650 µm)	Rare sub-angular and sub-rounded granites (200-900 µm), sub-rounded and rounded large basalt (200 µm- 1.2 mm) and andesite (250-800 µm)
Metamorphic Rock Fragments	n/a	n/a	n/a	n/a	n/a	n/a
Pyroxene (Ortho or clino)	Few orthopyroxene (100-300 µm) and clinopyroxene (augite 300-150 µm)	Rare clinopyroxene (augite) <90 µm and very rare orthopyroxene <300 µm	Orthopyroxene (100- 300 µm) and clinopyroxene (augite and rare diopside) (200-600 µm)	Ortho (100-350 µm) and frequent clinopyroxene (augite and very rare diopside) (150-300 µm)	Common orthopyroxene (70-300 µm) and rare clinopyroxene (augite) 150-300 µm	Rare orthopyroxene (100-300 µm) and clinopyroxene (augite and (150-400 µm)
Amphibole	Very rare, horneblende (euhedral), (150-300 µm)	n/a	Rare 150-340 µm	Very rare horneblende (100-400 µm).	Very rare	N/a
Mica	Very rare biotite crystals (50-250 µm)	n/a	Very rare biotite of medium dimension (150-500 µm).	Very rare biotite +/-300 µm.	Very rare	Rare biotite 50-300 µm
Quartz	30% sub-rounded, 70% sub-angular (50-500 µm).	50% sub–rounded, 50% sub-angular (130-50 µm) and few (150-200 µm).	30% sub-rounded, 70% sub-angular, (700-300 µm)- (50-200 µm).	% sub rounded 30 %sub-angular 70 (50-500 µm)	30% sub-rounded, 70% sub-angular, (50-500 µm)	30% sub-rounded, 70 %sub-angualr, (300-650 µm) -(50-250 µm).
Heavy minerals	Angular, sub-angular and sub-rounded (100-300 µm).	Rounded, sub-rounded and sub-angular (50-80 µm).	Sub-rounded and sub-angular (100-300 µm).	Sub-rounded and sub-angular (80-400 µm).	Rounded, sub-rounded and sub angular (90-350 µm).	Sub-rounded and sub-angular (100-300 µm).

Table 1. Summary of the petrographic analysis. (continued)

Group	Chontales A	Chontales B	Chontales C-1	Chontales C-2	Chontales D-1	Chontales D-2
K-feldspars	K-feldspars and plagioclase (150-500 µm), rare sanidine (450 µm).	K-feldspars and plagioclase, euhedral shape, angular and sub angular (50-250 µm).	K-feldspars and plagioclase, angular and sub angular. (100-450 µm).	K-feldspars and plagioclase (100-700 µm), angular and-sub angular.	K-feldspars and plagioclase, rare sanidine euhedral shape, angular and sub-angular. (150-600 µm).	K-feldspars and plagioclase (few large 700-1500 µm; average 150-500 µm), sanidine (700-1000), angular .and sub angular.
Olivine	Rare olivine (50-300 µm) and very rare iddingsite (100-150 µm).	Rare, +/- 50 µm.	Few, 50-250 µm; rare iddingsite.	Few, 50-300 µm.	Rare 150-500 µm.	Few, 50-400 µm.
Unknown	Hydrothermal alteration (150-350 µm).	Powdered granite with micropheno-crystals of olivine.	From no to rare hydrothermal alteration (200-250 µm).	Some cases of powdered granite with micropheno-crystals of olivine and hydrothermal alteration.	Hydrothermal alteration, in some cases in oolite shape. Powdered granite with micropheno-crystals of olivine.	Some cases of hydrothermal alteration (250-350 µm) and very rare powdered granite with micropheno-crystal of olivine.
Clay pellets	Rounded and sub-rounded clay pellets in various amounts (250-1300 µm).	Rounded clay pellets of significance dimensions (1,7 mm- 300 µm-750 µm).	Rare rounded and sub-rounded, 300-400 µm.	Rare rounded and sub-rounded (rare +/- 1.3mm and average 300-400 µm).	Rare rounded and sub-rounded, 200-700 µm.	N/a
Grog	Rare or not present (700 µm-2000 µm).	An isolate case in one sample, 600 µm.	From very rare to no examples (300-400 µm).	n/a	Few large grog fragments (400 µm -1500 µm).	Few large grog fragments (1100-1600 µm) and (400-500 µm).
Porosity	Mostly elongated voids, moderately oriented with the borders.	Long elongated voids and voids are both orientated with the borders.	Elongated, vugh and vescicle pores moderately oriented with the borders.	Elongated, vugh and vescicle pores, from moderately oriented with the borders to not oriented.	Elongate, vugh and vescicle pores from not oriented to moderately oriented.	Elongate, vughs and vescicles pores, moderately oriented with the borders.
Approx. Void Size (µm)	150-250 µm.	100-200 µm and some large cracks (600 µm-2000-3000 µm).	50-250 µm.	50-250 µm.	50-250 µm.	50-250 µm, in a few cases large 300-400 µm.
%paste	65-70%	0,8	60-65%	60-65%	65-70 %	65-70%

or rather, the presence of plagioclase, as well as carbonates. The high values in Fe are confirmed by the presence of orthopyroxene, basalt and iron-rich inclusions in samples AB-N-45, AB-L-78, and AB-L-68. These three samples were already grouped together in the petrographic analysis. A similar composition is also shown by the sherds in group Chontales D-1, which are characterised by a high correlation of Fe, Ti, and Ca. The first two elements are related to the presence of pyroxene minerals while calcium is associated with the plagioclase. Groups Chontales C-1 and C-2, in contrast to the previous groups (D-1 and D-2), are enriched in Sr. The lower value in Fe for samples AB-T-60 and AB-T-83Q can be linked to presence of granite and the low number of rock inclusions (e.g. andesite) and the total absence of basalt in contrast with other ceramic samples. For sample AB-E-68X, this low value can be connected to the matrix, which is characterised by a yellowish colour and considered an iron poor clay.

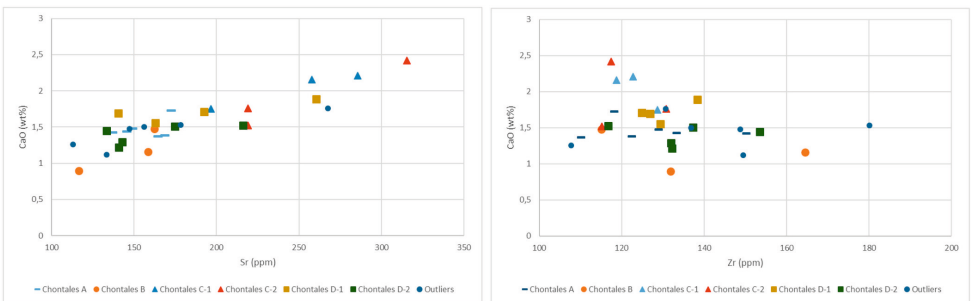

Figure 3. Biplot of CaO (wt.%) vs. Sr (ppm), CaO (wt.%) vs. Zr (ppm) values of the archaeological ceramics from Aguas Buenas M1. Samples are coloured according to the results of the petrographic analysis.

4. DISCUSSION

The correlation of the petrographic groups with the compositional analysis through the observation of single element values and element ratios was not unequivocal in attributing discrete sources. It is important to highlight that when such coarse grain ceramics are analysed together with the temper added during the manufacturing process, as in this case study, nonplastic inclusions may have a critical impact on the chemical composition results. The coarse grain size can obscure the presence of other minerals or the composition of the clay matrix which *in extremis* could influence the compositional results. It is thus essential that any potential problem is taken into account in discussing the p-XRF results. Multiple readings on each of the samples were collected in order to mitigate part of this potential variation, as the aim of the analysis is to delineate systematic differentiations within the ceramic assemblage.

Table 2. pXRF results of archaeological ceramics.

Macroscopic group	Group	Sample	CaO (wt%)	Fe_2O_3 (wt%)	TiO_2 (Wt%)	Sr (ppm)	Cr (ppm)	Zr (ppm)	Rb (ppm)	Nb (ppm)
AB-O	Chontales A	AB-O-71	1,4	9,1	1,2	137	n.d.	150	53	< 5
AB-C	Chontales A	AB-C-74A	1,4	10,3	1,3	164	73	110	61	< 5
AB-E	Chontales A	AB-E-68X	1,4	11,5	1,3	145	213	133	60	< 5
AB-F	Chontales A	AB-F-57	1,7	10,4	1,4	172	28	118	66	< 5
AB-O	Chontales A	AB-O-74	1,5	12	1,4	149	1	129	64	< 5
AB-I	Chontales A	AB-I-83	1,4	11,2	1,2	169	134	122	65	< 5
AB-T	Chontales B	AB-T-60	1,5	5,3	1	162	14	115	63	< 5
AB-T	Chontales B	AB-T-78A	0,9	3,1	0,8	117	35	132	70	< 5
AB-T	Chontales B	AB-T-83Q	1,2	3,3	0,7	159	127	165	68	< 5
AB-G	Chontales C-1	AB-G-71	2,2	9,9	1,3	286	16	123	61	< 5
AB-M	Chontales C-1	AB-M-71	1,8	11,3	1,4	197	145	129	60	< 5
AB-P	Chontales C-1	AB-P-71	2,2	10,8	1,6	258	96	119	57	< 5
AB-Q	Chontales C-2	AB-Q-89	1,8	9,6	1,1	219	n.d.	131	64	< 5
AB-N	Chontales C-2	AB-N-60	1,5	9,9	1,3	219	123	115	61	< 5
AB-A	Chontales C-2	AB-A-60	2,4	10,5	1,5	315	14	117	62	< 5
AB-D	Chontales D-1	AB-A-20	1,7	12,1	1,6	141	59	127	64	< 5
AB-A	Chontales D-1	AB-A-71Y	1,6	11,5	1,2	163	132	129	64	< 5
AB-M	Chontales D-1	AB-M-83	1,7	10,3	1,3	192	112	125	62	< 5
AB-H	Chontales D-1	AB-H-78	1,9	10,9	1,3	260	23	138	61	< 5
AB-B	Chontales D-2	AB-B-75	1,5	11,1	1,3	175	14	137	61	< 5
AB-H	Chontales D-2	AB-H-68	1,5	10,8	1,4	216	n.d.	117	58	< 5
AB-L	Chontales D-2	AB-L-68	1,2	10,7	1,1	141	76	132	66	< 5
AB-L	Chontales D-2	AB-L-78	1,3	10,6	1,3	143	84	132	69	< 5
AB-N	Chontales D-2	AB-N-45	1,4	10,3	1,2	133	39	153	66	< 5
AB-R	AB-R-74	AB-R-74	1,3	11,2	1,4	113	229	108	60	< 5
AB-S	AB-S-78	AB-S-78	1,8	10,7	1,3	268	213	131	61	< 5
AB-E	AB-E-68Y	AB-E-68Y	1,5	6	0,7	178	37	180	71	< 5
AB-F	AB-F-29	AB-F-29	1,1	11	1,3	133	30	149	54	< 5
AB-D	AB-D-29	AB-D-29	1,5	12	1,5	156	145	137	61	< 5
AB-D	AB-D-45	AB-D-45	1,5	7,2	0,9	147	76	149	64	< 5

Table 3. Average and standard deviation for the petrographic groups.

Standard deviation	CaO (wt%)	CaO (st. dev)	Fe_2O_3 (wt%)	Fe_2O_3 (st. dev)	TiO_2 (wt%)	TiO_2 (st. dev)	Sr (ppm)	Sr (st. dev)	Cr (ppm)	Cr (st. dev)	Zr (ppm)	Zr (st. dev)	Rb (ppm)	Rb (st. dev)	Nb (ppm)	Nb (st. dev)
Chontales A	1,5	0,1	10,8	0,9	1,3	0,1	156	13	69	77,1	127	12,7	62	4,4	< 5	0,5
Chontales B	1,2	0,2	3,9	1	0,9	0,1	145	20,7	58	48,9	137	20,5	67	3	< 5	1,7
Chontales C-1	2	0,2	10,7	0,6	1,4	0,1	246	37,2	85	53,2	123	4,1	60	1,7	< 5	0,5
Chontales C-2	1,9	0,4	10	0,4	1,3	0,1	251	45,4	29	55	121	6,9	62	1,4	< 5	0,9
Chontales D-1	1,7	0,1	11,2	0,7	1,3	0,1	189	45,1	81	43,2	129	5,2	63	1,4	< 5	0,5
Chontales D-2	1,4	0,1	10,7	0,3	1,3	0,1	162	30,8	35	33,1	134	11,8	64	4,1	< 5	0,7

The results of the clay survey of Casale et al. (2020) demonstrate how the majority of the suitable clay outcrops are located near the banks of rivers, as a result of fluvial sedimentation. It is likely that differential fluvial and alluvial depositional processes throughout the valley, which vary from seasonal streams to perennial rivers (such as the Mayales river), may have had an impact on, for example, the accumulation of Zr and by extent heavy minerals (such as zircon) (Degryse and Braekmans 2013). This results in a variable elemental composition within the raw materials employed for the preparation of the potterys. The scatter-plot of Ca and Sr (Fig. 3) shows that the two elements are partly correlated as expected, suggesting that the presence of Sr in the ceramics can be associated to both a microcrystalline (carbonate) composition of the raw materials, but more significantly relates to the feldspar component (and particularly plagioclase) of the fabric groups (Degryse and Braekmans 2013).

In order to successfully compare and integrate the analytical results of both clay and ceramic materials, we applied a multivariate statistical methodology for group assessment and variability. PCA and DA were calculated in SPSS using Fe_2O_3, CaO, TiO_2, Sr, Zr and Rb. Cr and Nb were not included to not mislead the interpretation of the calculation. The first has a high variability through the assemblage while the latter is present in very low quantity (on average < 5 ppm).

DA were determined to assess the validity of the ceramic groups created through the petrographic observations. Results demonstrated that 79.2% of the specimens were grouped correctly as with the petrography. Group C-1 has one sample (AB-G-71) that was assigned to C-2 and C-2 has one sample (AB-A-60) assigned to C-1. The same occurred with D-1 and D-2, where AB-A-71Y was assigned to D-2 and AB-H-68 was connected to D-1. Overall, the DA gave a positive result demonstrating that only five samples out of 30 were re-grouped differently, and four of that, were re-grouped between subgroups of the same main groups. Geochemical similarities are expected between subgroups of the same petrographic groups, due to the presence of similar mineral inclusions.

A PCA bivariate biplot was calculated including all samples, both reference clay data (n = 44) from Casale et al. (2020) and representative sherds (n = 30), in order to understand possible connections between the regionally available clay raw materials and ceramics from Aguas Buenas. An important result of the statistical calculation is that, in contrast with the two-elements plots, when more significant elements are analysed (Fe_2O_3, CaO, TiO_2, Sr, Zr, Rb), the petrographic groups identified show a consistent internal geochemical composition. Table 4 shows the results of the compositional analysis for the clay samples, the results of the grouping made by Casale et al. (2020), and the ceramics linked to the possible clay sources, following chemometric approach through PCA. Figure 4 graphically illustrates the comparison through PCA, in which both soil and ceramic samples are shown according to their compositional groups for clays and petrography for ceramics. The majority of the ceramic samples cluster together parallel

Table 4. p-XRF results for clay samples expressed in wt.% and ppm, together with the geographical coordinates (UTM, WGS84), extension and depth expressed in m for each clay outcrop, list of the clay samples clustered in groups according to PCA (Casale et al. 2020), and list of the petrographic groups of archaeological ceramics clustered to clay outcrops according to PCA.

Type of soil	Group	Sample	Petrographic group connections	CaO (wt%)	Fe2O3 (wt%)	TiO2 (Wt%)	Cr (ppm)	Sr (ppm)	Zr (ppm)	Rb (ppm)	Nb (ppm)	UTM_(E)	UTM_(N)	Visible Estimated Outcrop (m)	Sample Depth (m)
Arenoso/Barro	G1	ZA.1		4,8	16,8	2,2	295	160	112	62	7	672376	1342189	50x50	0,5-2
Barro_negro	G1	ZA.2		3,5	15,8	1,9	261	145	104	63	6	672862	1344023	1x10	0,2-0,5
Barro_amarillo	G1	ZA.3		3,4	15,5	2	234	158	99	56	7	672925	1343965	-	-
Barro_negro	G1	ZA.6		1,8	17,9	2,4	313	105	118	53	7	672925	1343965	-	-
Barro	G1	ZA.7		2,1	18,6	2,3	325	91	106	53	7	672774	1344018	-	-
Barro	G2	C3.1		2,1	9,5	1,1	152	308	130	67	< 5	674038	1334509	0x5	1
Barro	G2	D12.1	Chontales C-1, Chontales C-2	2,3	9,8	1	136	221	97	59	< 5	673761	1343369	3x10	>0,3
Barro_amarillo	G2	F12.3		2,3	10	1,2	103	368	127	64	< 5	673395	1341787	10x15	>1
Barro	G2	F4.1		2,6	11,4	1,3	155	305	78	58	< 5	674499	1334435	1x30	0-1,5
Barro	G2	F6.1		2,3	9	1	123	276	135	69	< 5	675376	1341229	10x20	2
Barro	G2	F6.3		2,6	11,3	1,2	279	333	108	63	< 5	674850	1341220	20x20	>0,2
Barro	G2	G6.1		2,6	9,8	1,1	358	445	81	64	< 5	675534	1341463	20x40	>0,3
Arenoso/Barro	G2	H2.2		2,6	11,9	1,2	143	353	88	60	< 5	677013	1334541	-	-
Barro_negro	G2	H2.3		2,8	12,2	1,2	164	329	81	61	< 5	676812	1334640	-	-
Barro	G2	H3.1		3,3	12,7	1,4	327	402	79	60	< 5	676962	1342742	5x400	>1
Barro	G2	H3.2		2,5	13,6	1,6	458	376	87	60	< 5	677206	1340460	25x25	5-6m
Arenoso/Barro	G2	H5.1		3,5	11,2	1,3	279	457	86	60	< 5	677347	1340986	30x2	-
Barro_negro	G2	I11.1		2,2	14,1	1,3	390	267	73	56	< 5	677641	1335321	10x10	0,5
Barro/Barrial	G2	M3.1	Chontales C-2, Chontales D-1, Chontales D-2	1,9	11	1,2	123	192	99	66	< 5	677640	1335322	10x10	0,5-0,7
Barro	G2	M3.2	Chontales A, Chontales D-1, Chontales D-2	1,4	12,7	1,3	171	129	109	69	< 5	677481	1340619	2x5	1
Barro	G2	N3.1		1,9	10	1,1	216	221	117	71	< 5	679278	1344248	-	-

Table 4. p-XRF results for clay samples expressed in wt.% and ppm, together with the geographical coordinates (UTM, WGS84), extension and depth expressed in m for each clay outcrop, list of the clay samples clustered in groups according to PCA (Casale et al. 2020), and list of the petrographic groups of archaeological ceramics clustered to clay outcrops according to PCA. (continued)

Type of soil	Group	Sample	Petrographic group connections	CaO (wt%)	Fe2O3 (wt%)	TiO2 (Wt%)	Cr (ppm)	Sr (ppm)	Zr (ppm)	Rb (ppm)	Nb (ppm)	UTM_(E)	UTM_(N)	Visible Estimated Outcrop (m)	Sample Depth (m)
Barro	G2	N4.2	Chontales C-2, Chontales D-1, Chontales D-2	2,3	9,1	1,1	141	149	96	57	< 5	679323	1344707	-	-
Barro/Barrial	G3	B2.4		2,1	3,9	0,6	26	382	173	66	< 5	679071	1343650	2x3	0,5-1
Arenoso/Barro	G3	C12.1	Chontales C-1, Chontales C-2	2,5	9,2	1	46	264	89	58	< 5	679143	1343647	2x10	0,5-1
Barro	G3	C5.1		2,2	7	1	37	347	154	72	< 5	678730	1341642	50x50	2
Barro	G3	D5.1		2,5	8,4	1,1	35	337	111	69	< 5	678738	1339413	5x10	-
Barro	G3	D5.2		1,9	10	1,2	37	296	122	69	< 5	680115	1345503	10x30	0,2-1
Barro	G3	E5.1	Chontales C-1, Chontales C-2	2	9,9	1,2	68	337	115	63	< 5	680170	1339736	1x2	1
Barro_amarillo	G3	F12.1		2,4	10	1,2	35	352	117	63	< 5	680168	1339732	2x10	1
Barro	G3	G11.2		2,3	9,9	1,1	69	272	138	71	< 5	680280	1339717	2x10	1
Barro	G3	H7.1		2,4	9,4	1,2	n.d.	308	138	64	< 5	680915	1341320	10x20	0-1
Barro	G3	I7.1		2	7,8	0,9	84	227	132	73	< 5	680719	1339423	5x10	0,2-1,2
Barro	G3	I7.2		2	8	1	73	194	127	72	< 5	682161	1344172	5x10	0,25-0,6
Barro	G3	L5.2		3,4	8,4	1	64	312	99	76	< 5	681898	1343234	100x100	0,1-0,2
Barro	G3	L7.1		1,8	10,6	1,2	75	252	108	72	< 5	681871	1343310	50x50	0,20-0,40
Barro	G3	M2.1		2,6	10,3	1,1	68	337	89	62	< 5	683424	1343871	10x50	> 0,3
Barro/Barrial	G3	O5.1		1,6	8,3	1,1	14	218	143	66	< 5	683436	1342528	1x10	0,25
Barro	G4	A4.2		2,3	5,8	1,2	n.d.	417	153	69	< 5	684135	1341858	2x10	0,2-0,25
Barro	G4	B2.5		1,6	3,9	0,4	n.d.	127	204	88	< 5	623088	1300805	0,5x1	0,4
Barro	G4	B2.6		1,3	3,9	0,5	n.d.	190	195	73	< 5	624006	1301271	0,5x10	0,2
Barro	G4	B2.7		1,7	3,6	0,5	n.d.	129	213	96	< 5	624094	1301410	0,5x2	0,1
Barro_amarillo	G4	G11.3		2,3	9,9	1,2	n.d.	267	138	69	< 5	623995	1300892	1x10	0,2-0,6
Barro	G4	I7.3		1,5	8,4	1,1	n.d.	243	142	78	< 5	624119	1301006	0,5x5	0,1-0,5

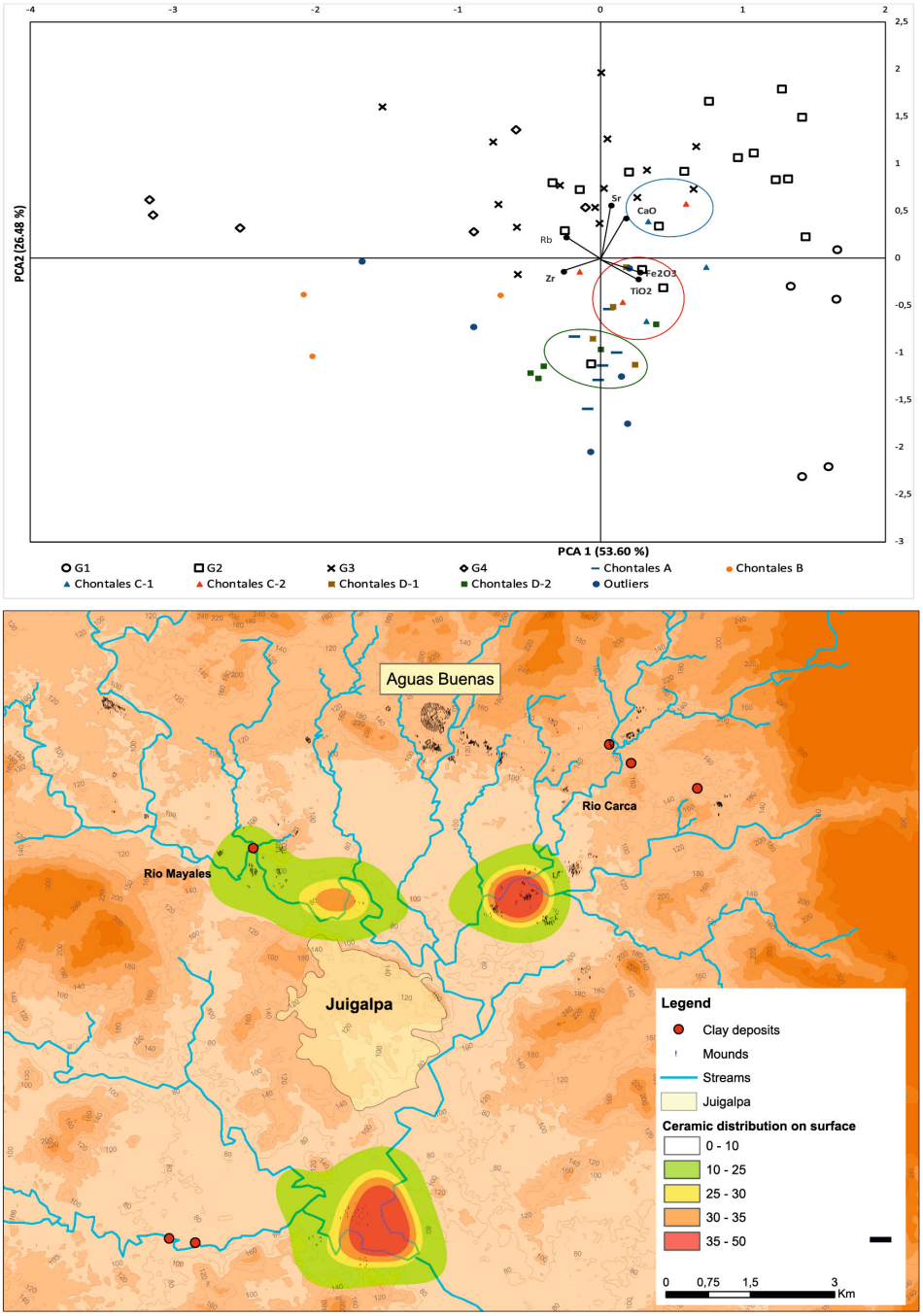

Figure 4. At the top combined PCA results of clay samples and archaeological ceramics. Each colour represents one of the four compositional groups identified with the PCA for clays (Casale et al. 2020) and the six petrographic groups for ceramics. At the bottom Geographic distribution of clay samples associated to Aguas Buenas (reddots) combined with the distribution of mounds (smaller black dots) and different intensities of surface ceramics.

to petrographic grouping but diverging from some of the clay outcrops analysed. Overall, petrographic and chemical data of the ceramics provides consistent observations and confirm the presence of different resource areas. In order to further test the reliability of the groups identified in PCA, Squared Mahalanobis distances were calculated to assess predicted and statistically assigned groups. Results indicated that 75% of the ceramics and clays were assigned to the same clusters as those evidenced in PCA. Generally, some overlap exists between Chontales A, D-1 and D-2 arguing for chemically related clay outcrops which can however be clearly separated through optical microscopy. Chontales B is clearly discerned from the rest of the ceramics, both mineralogically as well as chemically. Chontales C1 and C2 on the other hand overlap more significantly and can be considered chemically consistent which suggests the difference between C-1 and C-2 would be rather production related.

A positive attribution can be made for six clays outcrops (D12.1, E5.1, M3.2, M3.1, C12.1 and N4.1) which cluster with 13 ceramics in three major groups. These results propose that some of the ceramics retrieved in Aguas Buenas were likely produced with local clay readily available in the surrounding environment. The outcrop M3.2 matched seven ceramics from Chontales A (AB-E-68X, AB-O-74, AB-I-83), Chontales D-1 (AB-A-20, AB-A-71Y) and Chontales D-2 (AB-B-75, AB-L-68), while N4.2 and M3.1 clustered with Chontales C-2 (AB-N-60), Chontales D-1 (AB-M-83). The clays samples D12.1 and C12.1 matched with AB-G-71 and AB-A-60 from petrographic groups Chontales C-1 and C-2.

Generally, both ceramics and clays yielded low-calcareous crystalline matrices associated with basalt and andesite parent rocks. Figure 4 shows the resulting geographic distribution of clay samples that were associated with Aguas Buenas` ceramics, together with the location of the other mounds in the valley, and the locations that yielded surface ceramic materials. Table 4 lists these associations of the ceramic samples with the corresponding mineral resources. Regarding the mineral resources, Group 1 (G1) includes only the (clay) samples from the Zapatera Island, yielding systematic higher values of TiO_2, Cr, and Fe_2O_3, in contrast to the other groups. DA considers this group independent from the rest of the assemblage with 100% of correctness. The Zapatera Island is a shield volcano, which is characterized by basaltic/andesitic rocks and the Fe_2O_3 contents can be connected to mafic minerals such as pyroxenes, biotite and olivine which characterized the landscape. These clay samples cluster outside any other groups, suggesting these can be positively discriminated and thus that the ceramics recovered at Aguas Buenas were not manufactured with clays from the island.

Different technological practices are identified as well. Chontales B, for instance, has the finest matrix in the assemblage. The fine size of the inclusions can be the result of sieving practices that eliminated coarse grains affecting the final geochemical composition and workability of the matrix, which strongly diverge from the rest of the assemblage. Recent observations have connected these finds as part of the Sulaco

valley technical complex in northeastern Honduras (R. A. Joyce, personal communication, October 2019), which would further explain not only the wide difference in petrographic and geochemical values, but also in aesthetic perceptions. Petrographic groups Chontales C (C-1 and C-2) as well as Chontales D (D-1 and D-2) show a similar internal chemical composition as demonstrated by PCA and DA, supporting the petrographic observations.

Looking at the extension of the clay outcrops, the clay deposits that yielded the highest similarity with the archaeological ceramics (M3.2, M3.1, D12.1, C12.1, N4.2, E5.1) are also the largest in extension (Casale 2017; Casale et al. 2020). It is indeed likely that populations in pre-Hispanic times quarried those sources, although a more precise identification of specific outcrops along this river system, or its tributary streams and creeks, is currently not possible.

Furthermore, the combination of data regarding clay outcrops location and specific archaeological site location in the valley provides interesting data that clarify on human-landscape interaction and mobility. Each clay outcrop has archaeological sites in the vicinity, often within less than 2 km (Fig. 4). However, these sites were not contemporaneous to Aguas Buenas, dating to a later period (Donner and Geurds 2018). This enables further studies on the ceramic materials retrieved from these sites, and to understand possible connections with Aguas Buenas.

Consequently, the differences in sizes between documented exposed clay areas seem to be relevant in clay procurement choices. If we consider a long-term use of these natural resources, then it is possible that inhabitants of the area looked for the largest and perhaps the most sustainable sources available, in order not to rapidly exhaust them (Arnold 2000). Large quarries were not employed for massive production, since we have no evidence for such manufacturing practices in the history of the subbasin. Therefore, we can also propose that the selection of larger deposits ensured the continuity of socially learnt clay procurement practices over time. Such use strategies were likely shared among different communities of practitioners.

The optical microscopy analysis outlines the presence of different paste groups and, in some cases, the technological choice of mixing more than one clay for producing vessels. Clay mixing can be due to several reasons, from simple habit to liquidating older supplies (Gosselain and Livingstone-Smith 2005), but mixing can also aid in achieving specific desired features such as plasticity, firing resistance and/or dimension of the pots (Arnold 2000, Rice 1987; Albero Santacreu 2014, Michelaki, Braun and Hancock 2015). In order to control these features, potters can mix different clay sources for improved results. The compositional and petrographic analyses show that there are some pots consistently made with more fine grains (such as AB-T-78A, AB-T-60, AB-T-83Q), and others with coarser grains (for instance Chontales D-1 and D-2).

Clay outcrop M3.1 is the closer one to Aguas Buenas (< 3 km), has the largest surface area (100 x 100 m), and also matches other samples, although to a lesser extent. Outcrop N4.2 is located at less than 1 km distance from outcrop M3.1 and approximately 5 km from Aguas Buenas, suggesting the possibility of mixing more clays to reach a better workability of the paste, as was highlighted by the petrographic observation specifically for groups Chontales D-1 and Chontales D-2. Therefore, clays from M3.1 and N4.2 may have been employed by the population and strategically mixed with other clays, or tempered, reflecting different technological choices and production practices.

5. CONCLUSIONS

Since 2009, the detailed archaeological investigation of the Aguas Buenas monumental site by the *Proyecto Arqueológico Centro de Nicaragua* (directed by Geurds), and its relatively unique form and dimensions, has opened a range of questions concerning the sites' construction, associated practices and wider importance in the Mayales subbasin. As part of this corpus of studies, we have here analysed practices related to clay procurement and pottery-making, using mineralogical and geochemical methods. The integration of both optical microscopy with non-destructive XRF analysis provided the necessary basis for building an interpretative framework for provenance. The petrographic analysis demonstrates that, even when excavating a single mound (M1) and within a similar volcanic geological substrate, sherds show considerable mineralogical differences, leading to clear divisions into different provenance groups. The further use of the p-XRF as a connected chemical field method, confirmed the presence of systematic compositional groups. Results are promising and suggest the existence of ceramic materials that were manufactured with raw clays from diverse local origins as well as materials produced with clays from outside the Rio Mayales subbasin. The statistical analysis indicates that six clay outcrops, compositionally matching the ceramics from Mound M1 at Aguas Buenas, are located near other clusters of mounds, zones of high-intensity surface ceramics, but mostly with larger clay deposits also being available nearby. In particular, the results show that, even though there are suitable clay outcrops within a 1 km radius of the site (Casale et al 2020), raw materials are chosen from outcrops between 3 and 5 km away. This is relevant when considering the people that built Aguas Buenas, and their relationship to the surrounding landscape. The exploitation of several raw material sources simultaneously, for example, implies a detailed knowledge of the territory, as well as pointing to several different groups engaged with pottery-making activities.

The methodological framework entailed a combination of petrographic and compositional analysis of ceramic materials and clay samples, generating information

to support a number of conclusions about the nature of the pre-Hispanic Aguas Buenas site and its role among people living throughout the Mayales river subbasin. Also, it shows variability in pottery production operational sequences, from clay procurement –andesitic vs. basaltic clays–, clay preparation–tempering, mixing, and sieving practices–to surface treatment–smoothing and slipping gestures.

It is likely that additional systematic and large-scale archaeometric analysis based on, for example, more high resolution compositional techniques (such as for example XRD, INAA, and ICP-MS), applied to cultural materials from sites spanning the entire subbasin, will further clarify the extent of connectivity between groups in central Nicaragua. XRD analysis, for instance, allows to characterize the presence of different clays in the same ceramic body, clarifying further on the technology and clay preparation strategies. Ultimately, this research provides a first framework of investigation that can be employed in future extensive studies on the Mayales river subbasin, and the chosen methodology holds potential for its application in other regions as well.

Acknowledgments

We would like to thank Kaz van Dijk, Gabriel van der Pluijm, and Pol Miguel Salles for their invaluable assistance during fieldwork. Also, we are indebted to Leontien Talboom, who assisted in the survey, and built the database that was used in the laboratory. We gratefully acknowledge the aid of Alejandro Arteaga Saucedo, who provided relevant data that made the design of the maps possible. We express our gratitude to the Nicaraguan Institute of Culture, and in particular its co-director Luis Morales Alonso and the director of the Archaeology Directorate, Ivonne del Carmen Miranda Tapia, for their continued support of the project, and for issuing the permits to export samples. The Archaeological Museum Gregorio Aguilar Barea in Juigalpa was very supportive in the early stages leading up to this research. We are also indebted to Loe Jacobs and Eric Mulder for their enthusiasm and relentless help at the Laboratory for Artefact Studies at the Faculty of Archaeology, Leiden University. Finally, the clay survey was greatly facilitated by Eleucterio Castillo, our local guide and friend, whose key knowledge of the landscape and the communities proved vital. Finally, we would like to thank the three anonymous reviewers for their constructive suggestions to improve this paper.

Funding: This research was made possible by the Netherlands Organisation for Scientific Research (NWO) VIDI grant “Networked practices of contact: Cultural identity at the Late prehistoric settlement of Aguas Buenas, Nicaragua, AD 500–1522” (PI Alexander Geurds).

REFERENCES

Albero Santacreu, D. (2014). Materiality, Techniques and Society in Pottery Production: The Technological Study of Archaeological Ceramics Through Paste Analysis. Warsaw/ Berlin: De Gruyter Open Ltd.

Arengi, J. T., Hodgson, G. V. (2000). Overview of the Geology and Mineral Industry of Nicaragua. International Geology Review, 42(1), 45-63.

Arnold, D. E. (2000). Does Standardization of Ceramic Pastes Really Mean Specialization? Journal of Archaeological Method and Theory, 7, 333-375.

Arteaga S., A. (2017). Reconstrucción del paisaje social prehispánico en la microcuenca del río Mayales, Chontales, Nicaragua. Unpublished Master thesis, Universidad Nacional Autónoma de México.

Auzina, D. (2018). Monumentality by Communities. Mapping the Spatial Logic of the Pre-Hispanic Site Aguas Buenas (AD 400-1600) in Central Nicaragua. Research Master thesis, Leiden University.

Abzalov, M. (2008). Quality Control of Assay Data: A Review of Procedures for Measuring and Monitoring Precision and Accuracy. Exploration and Mining Geology, 17(3-4):131–144.

Baxter, M. (2003). Statistics in Archaeology. London: Hodder Arnold.

Braekmans D. and Degryse P. (2016). Petrography: Optical Microscopy. In: A. Hunt (ed.) The Oxford Handbook of

Archaeological Ceramic Analysis, Oxford University Press, Oxford, p233-265.

Casale, S. (2017). Pre-hispanic clay roads. Evaluation and interpretation of ceramic products and raw clay procurement in the Rio Mayales Subbasin, Chontales, Nicaragua. Research Master thesis, Leiden University.

Casale, S., Donner, N. R., Braekmans, D., Geurds, A. (2020). Pre-Hispanic and contemporary raw materials use in earthenware production in the Río Mayales subbasin, Chontales, central Nicaragua. In Klinkenberg, V., R. van Oosten and C. van Driel-Murray (eds.). A Human Environment. Studies in honour of 20 years Analecta editorship by Prof. Dr. Corrie Bakels. Analecta Praehistorica Leidensia (APL) 50. Leiden: Sidestone Press. ISBN 978-90-8890-906-1

Donner N. R., Arteaga A., Geurds A. & Dijk K. van (2018). Caracterización inicial de los sitios arqueológicos en la subcuenca del río Mayales, Departamento de Chontales, Nicaragua. Cuadernos de Antropología 28(1): 1–26

Donner, N. R., Geurds, A. (2018). The valley of Juigalpa, Mayales River Sub-basin Microregion (Chontales, Nicaragua) Date list I. Radiocarbon 60(2), 1-10.

Degryse, P., Braekmans, D. (2013). Elemental and Isotopic Analysis of Ancient Ceramics and Glass. In H. H. Turekian, Treatise on geochemistry (Vols. 2nd Edition, vol. 14, 191-207). Oxford: Elsevier.

Emmitt, J.J., McAlister, A.J., Phillipps, R.S., Holdaway, S.J., (2018). Sourcing without sources: Measuring ceramic variability with pXRF. Journal of Archaeological Science: Reports, 17, 422-432.

Finlay, A., McComish, J., Ottley, C., Bates, C., Selby, D. (2012). Trace element fingerprinting of ceramic building material from Carpow and York Roman fortresses manufactured by the VI Legion. Journal of Archaeological Science, 39 (7), 2385-2391

Frahm, E. (2018). Ceramic studies using portable XRF: From experimental tempered ceramics to imports and imitations at Tell Mozan, Syria. Journal of Archaeological Science, 90, 12–38.

Garayar, J. (1972). Geología y depósitos de minerales de la región de Chontales y Boaco. Catastro y Reservas Minerales, División de Geología, Informe, (11), Managua.

Geurds, A. (2010). Proyecto Arqueológico Centro de Nicaragua. Temporadas 2010-11 El Ayote-RAAS. Unpublished report, INC, Managua.

Geurds, A. (2012). Proyecto arqueológico Centro de Nicaragua. Temporada 2012. Informe Tecnico Final. Unpublished report, INC, Managua.

Geurds, A. (2013). Proyecto Arqueológico Centro de Nicaragua. Temporada mayo-junio, 2013. Informe. Unpublished report, INC, Managua.

Geurds, A. (2014). Proyecto Arqueológico Centro de Nicaragua (PACEN). Séptima etapa: prospección intensiva, mapeo total y excavación en sitio Aguas Buenas (cuarta temporada), comarca San Isidro, Juigalpa, Chontales. Unpublished report, INC, Managua.

Geurds, A., Donner, N. R., Arteaga, A., Angeles, R., Torreggiani, I., Donner, D., Ayala L., A., Mendoza C., L., Murguia L., J. (2015). Reporte Preliminar Proyecto Arqueológico Centro de Nicaragua (PACEN) Novena etapa. Unpublished report, INC, Managua.

Geurds, A., Terpstra, D. (2017). Circular Reasoning in Mound Building? Large- scale Planned Construction Patterns at the Aguas Buenas Site (A.D. 400–1525). In: War & Peace: Conflict and Resolution in Archaeology (pp. 47–59). Proceedings of the 45th Annual Chacmool Archaeology Conference, edited by Adam K. Benfer. Chacmool Archaeology Association, University of Calgary, Calgary, Alberta, CA.

Glascock, M. D., Neff, H., Stryker, K. S., Johnson, T. N. (1994). Sourcing archaeological obsidian by an abbreviated NAA procedure. J. Radioanal. Nucl. Chem., 180 (1), 29–35.

Gratuze, B., 1999. Obsidian characterization by laser ablation ICP-MS and its application to prehistoric trade in the Mediterranean and the Near East: sources and distribution of obsidian within the Aegean and Anatolia. J. Archaeol. Sci. 26 (8), 869–881.

Gorin, F. (1990). Archéologie de Chontales, Nicaragua (3 vols.). Dissertation, Université de Paris I, Paris.

Gosselain, O. P., Livingston-Smith, A. (2005). The source: Clay selection and processing practices in sub-Saharan Africa. In: Livingston-Smith, Bosquet, A., Martineau, D. (Eds), Pottery manufacturing processes:reconstitution and interpretation. Acts of the XIVth UISPP Congress, University of Liége, Belgium, 2–8 September 2001. Oxford: BAR-IS 1349(2005) 33–47.

Guerra, M.F., 1998. Analysis of archaeological metals. The place of XRF and PIXE in the determination of technology and provenance. X-Ray Spectrometry 27, 73-80.

Hradecký, P. (2011). Introduction to the special volume "Subduction-related igneous activity in Central America – Its nature, causes and consequences". Journal of Geosciences 56 (1): 1-7.

Hughes, R.E., Högberg, A., Olausson, D. 2010. Sourcing flint from Sweden and Denmark: a pilot study employing non-destructive energy dispersive X-ray fluorescence spectrometry. Journal of Nordic Archaeological Science 17, 15-25.

Hunt, A. M. W., Speakman, R. J. (2015). Portable XRF analysis of archaeological sediments and ceramics. Journal of Archaeological Sciences, 53, 626–638.

Michelaki, K., Braun, G. V., Hancock, R. G. V. (2015). Local Clay Sources as Histories of Human–Landscape Interactions: a Ceramic Taskscape Perspective. Journal of Archaeological Method and Theory, 22(3), 783-827.

Morgenstein, M., Redmount, C. A. (2005). Using portable energy dispersive X-ray fluorescence (EDXRF) analysis for on-site study of ceramic sherds at El Hibeh, Egypt. Journal of Archaeological Science, 32, 1613–1623.

Orton, C., & Hughes, M. (2013). Pottery in Archaeology. New York: Cambridge University Press.

Pincé, P., Braekmans, D., Abdali, N., De Pauw, E., Amelirad, S., Vandenabeele, P. (2018). Development of ceramic production in the Kur River Basin (Fars, Iran) during the Neolithic. A compositional and technological approach using X-ray fluorescence spectroscopy and thin section petrography. Archaeological and Anthropological Sciences, 1-18.

Quinn, P. S. (2013). Ceramic Petrography: The Interpretation of Archaeological Pottery & Related Artefacts in Thin Section. Oxford: Archaeopress.

Rice, P. M. (1987). Pottery analysis: A sourcebook. Chicago: University of Chicago Press.

Rigat, D. (1992). Préhistoire au Nicaragua: Région Juigalpa Vol 3. Dissertation, University of Paris.

Sharrat, N., Golitko, M., Williams, P.R., Dussubieux, L. (2009). Ceramic Production during the Middle Horizon: Wari and Tiwanaku Clay Procurement in the Moquegua Valley, Peru. Geoarchaeology 24(6), 792-820.

Shugar, A., Mass, L. (2012). Handheld XRF for Art and Archaeology. Vol. 3. Leuven: Leuven University Press

Speakman, R.J., Little, N.C., Creel, D., Miller, M. R., Iñañez, J. G. 2011. Sourcing ceramics with portable XRF spectrometers? A comparison with INAA using Mimbres pottery from the American Southwest, Journal of Archaeological Science 38 (12), pp. 3483-3496.

VanDerwarker, A. M. and Marcoux, J. B. (2019). Principal Component Analysis. In The Encyclopedia of Archaeological Sciences, S. L. López Varela (Ed.). doi:10.1002/9781119188230.saseas0477

Vlaskamp R. J. C., Geurds A., Jansen R. (2014). Reporte de las investigaciones arqueológicas entre 2011–2014 en el sitio prehispánico de Aguas Buenas, Chontales, Nicaragua. Mi Museo y Vos 8(29), 6–12.

Weigand P. C., Harbottle G., Sayre, E.V. (1977). Turquoise sources and source analysis: Mesoamerica and the Southwestern USA. In: Earle TK and Ericson JE (eds.), Exchange Systems in Prehistory (pp. 15–34). New York: Academic Press.

Wronkiewicz D. J. and Condie K. C. (1987) Geochemistry of Archean shales from the Witwatersrand Supergroup, South Africa: Source-area weathering and provenance. Geochimica et Cosmochimica Acta, 51, 2401–2416.

Table S1. Certified versus measured values of reference materials. including percent relative difference (% RD) (n.d. not determined).

	98b			**GSP-2**			**BIR-1a**			**CRM667**			**SGR-1b**		
	certified	measured	% RD	certified	measured	% RD	certified	measured	% RD	certified	measured	% RD	certified	measured	%RD
K_2O (wt.%)	3.38	3.46	2.41	5.38	5.11	5.06	0.03	n.d.	-	n.d.	-	-	1.66	1.8	7.89
CaO (wt.%)	0.11	0.14	25.88	2.1	1.9	10.26	13.3	12.46	6.48	n.d.	-	-	8.38	8.95	6.54
TiO_2 (wt.%)	1.35	1.41	4.42	0.66	0.67	1.77	0.96	1.02	6.51	n.d.	-	-	0.24	0.27	13.01
Fe_2O_3 (T) (wt.%)	1.69	1.59	5.79	4.9	4.52	8.11	11.3	10.81	4.44	6.41	6.58	2.68	3.03	3.09	1.9
Zn (ppm)	110	103	6.49	120	111	7.51	70	68	2.24	175	141	21.2	74	83	11.97
Ni (ppm)	n.d.	-	-	17	13	27.14	170	117	37.13	128	143	11.16	29	31	6.88
Rb (ppm)	180	178	1.24	245	230	6.35	n.d.	-	-	n.d.	-	-	n.d.	-	-
Sr (ppm)	189	195	3.06	240	226	5.95	110	112	2.06	206-243	204	8.66	420	410	2.32
Y (ppm)	n.d.	-	-	28	n.d	-	16	-	-	16.7-25.3	-	-	13	-	-
Zr (ppm)	220	231	4.89	550	517	6.24	18	14	23.78	n.d.	-	-	53	55	3.2
Nb (ppm)	n.d.	-	-	27	24	9.99	0.6	-	-	n.d.	-	-	5	-	-
Cr (ppm)	119	127	6.82	20	23	14.37	370	352	5.08	178	190	6.52	30	34	11.1

Table S2. Number of cases predicted and assigned to each of the petrographic groups based on discriminant analysis using Mahalanobis distances.

Classification Results: 79.2% of original grouped cases correctly classified.									
			Predicted Group Membership						**Total**
Groups			**1**	**2**	**3**	**4**	**5**	**6**	
Original	Count	1 - Chontales A	5	0	0	0	0	1	6
		2 - Chontales B	0	3	0	0	0	0	3
		3 - Chontales C-1	0	0	1	1	1	0	3
		4 - Chontales C-2	0	0	1	2	0	0	3
		5 - Chontales D-1	1	0	0	0	3	0	4
		6 - Chontales D-2	0	0	0	0	0	5	5
	%	1 - Chontales A	83.3	0	0	0	0	16.7	100
		2 - Chontales B	0	100	0	0	0	0	100
		3 - Chontales C-1	0	0	33.3	33.3	33.3	0	100
		4 - Chontales C-2	0	0	33.3	66.7	0	0	100
		5 - Chontales D-1	25	0	0	0	75	0	100
		6 - Chontales D-2	0	0	0	0	0	100	100

Table S3. Ceramic and clay samples grouped according to PCA and the predicted groups following the DA analysis. Statistical differences for group attribution are indicated with **.

Sample code	Prior PCA group	Predicted DA group	Sample code	Prior PCA group	Predicted DA group
ZA.1	1	1	**F12.1**	**3**	**2****
Za.2	1	1	G11.2	3	3
ZA.3	1	1	**H7.1**	**3**	**5****
ZA.6	1	1	I7.1	3	3
ZA.7	1	1	I7.2	3	3
C3.1	**2**	**3****	L5.2	3	3
D12.1	5	5	L7.1	3	3
F12.3	2	2	**M2.1**	**3**	**2****
F6.1	**2**	**3****	**O5.1**	**3**	**7****
F6.3	2	2	A4.2	4	4
G6.1	2	2	B2.5	4	4
H2.2	2	2	B2.6	4	4
H2.3	2	2	B2.7	4	4
H3.2	2	2	**G11.3**	**4**	**3****
H5.1	2	2	I7.3	4	4
M3.2	6	6	**AB-C-74A**	**6**	**7****
N3.1	**2**	**3****	AB-E-68X	6	6
N4.2	7	7	AB-O-74	6	6
F4.1	**2**	**5****	AB-I-83	6	6
H3.1	2	2	AB-G-71	5	5
I11.1	2	2	AB-N-60	7	7
M3.1	7	7	AB-A-60	5	5
B2.4	**3**	**4****	AB-A-20	6	6
C12.1	5	5	AB-A-71Y	6	6
C5.1	3	3	AB-M-83	7	7
D5.1	3	3	**AB-H-78**	**7**	**5****
D5.2	3	3	AB-B-75	6	6
E5.1	**5**	**3****	**AB-L-68**	**7**	**6****